THE JOURNAL OF PHYSICAL CHEMISTRY B

Article

pubs.acs.org/JPCB

Accelerated Particle-Based Target Capture—The Roles of Volume Transport and Near-Surface Alignment

Alexander van Reenen,[†,*] Arthur M. de Jong,[†] and Menno W. J. Prins[†,‡]

[†]Eindhoven University of Technology, Eindhoven, The Netherlands

[‡]Philips Research, Eindhoven, The Netherlands

Supporting Information

ABSTRACT: The upcoming generations of high-sensitive and miniaturized biosensing systems need target capture methods that are as efficient and as rapid as possible, with targets ranging from molecules to cells. Capture of the targets can be achieved using particles coated with affinity molecules, but there are still fundamental questions as to the processes that limit the association rates. In this paper we quantify and compare the reaction rates of particle-based target capture with different types of actuation, namely (i) passive thermal transport, (ii) fluid agitation by vortex mixing, and (iii) actively rotating particles. In the experiments, we use fluorescent nanoparticles as targets which are biochemically captured by magnetic microparticles, and the capture efficiency is quantified using fluorescence microscopy with single target resolution. The data unravel the contributions of volume transport, near-surface alignment, and the chemical reaction to the overall rate constant of association. Vortex mixing versus passive transport gives an increase of the reaction rate constant by more than an order of magnitude, implying that the encounter frequency as well as the near-surface alignment probability are increased. The importance of near-surface alignment is underscored by the data of active particle rotation; the binding probability per encounter is 4-fold enhanced on rotating capture particles. We discuss the implications of our results for different biological systems and for the development of novel actuation methods in particle-based target capture.

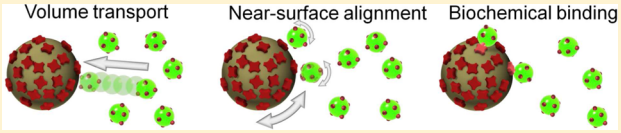

INTRODUCTION

Affinity molecules are widely used for the capture and extraction of specific targets from a biological sample, e.g., cells, proteins, or nucleic acids. The affinity molecules are generally immobilized on a solid carrier, and the targets are captured from the fluid onto the carrier by specific binding to the affinity molecules. In many assay systems, magnetic micro- or nanoparticles are used as carriers for the affinity molecules, because magnetic particles have a high surface-to-volume ratio, are mobile in the fluid, and can be manipulated by magnetic fields. Applications range from cell extraction,[1,2] immunoassays,[3−5] nucleic-acid extraction,[6,7] to the latest ultrahigh-sensitivity affinity assays which count target molecules with single-molecule resolution.[8,9] Ultrahigh-sensitivity affinity assays are particularly challenging when the biological targets are to be captured from a small sample volume. In small samples only very few targets are available in the assay and the assay precision becomes limited by counting statistics, so every single target needs to be captured from solution and the capturing effectiveness needs to be close to unity.

In this paper, we investigate the processes that limit the association rate in particle-based target capture, to lay the foundation for novel particle-based target capture methods for small sample volumes. We describe a theoretical framework and experiments that separate the processes of volume transport, near-surface alignment, and the chemical binding reaction (see Figure 1a). In the experiments the capture of fluorescent target particles (FT) by magnetic capture particles (MC) is recorded with single-target resolution as a function of time, which gives the overall target capture rate. In order to unravel the contributions of volume and near-surface transport, we report and analyze experiments with fluid agitation and experiments with magnetic particle rotation, using passive target capture as the reference (see Figure 1b). In the Conclusion, we will discuss the implications of our results for the capturing of different biological targets (from molecular biomarkers to biological cells) and for the development of novel actuation methods in microfluidic particle-based affinity capture.

THEORETICAL CONSIDERATIONS

We model the capture of fluorescent target particles (FT) by magnetic capture particles (MC) in analogy to a bimolecular binding process.[10−12] Such a process is usually considered to consist of a (diffusional) encounter step and a subsequent intramolecular chemical reaction to obtain the bound complex (FTMC):

$$\mathrm{FT} + \mathrm{MC} \underset{k_{\mathrm{sep}}}{\overset{k_{\mathrm{enc}}}{\rightleftarrows}} \mathrm{FT}\cdots\mathrm{MC} \underset{k_{-c}}{\overset{k_c}{\rightleftarrows}} \mathrm{FTMC} \quad (1)$$

with k_{enc} the encounter rate constant, k_{sep} the separation rate constant, k_c the rate constant for complex formation, and k_{-c} the rate of decomplexation. The intermediate state, FT···MC,

Received: August 8, 2012
Revised: December 12, 2012
Published: January 8, 2013

dx.doi.org/10.1021/jp307862h | J. Phys. Chem. B 2013, 117, 1210−1218

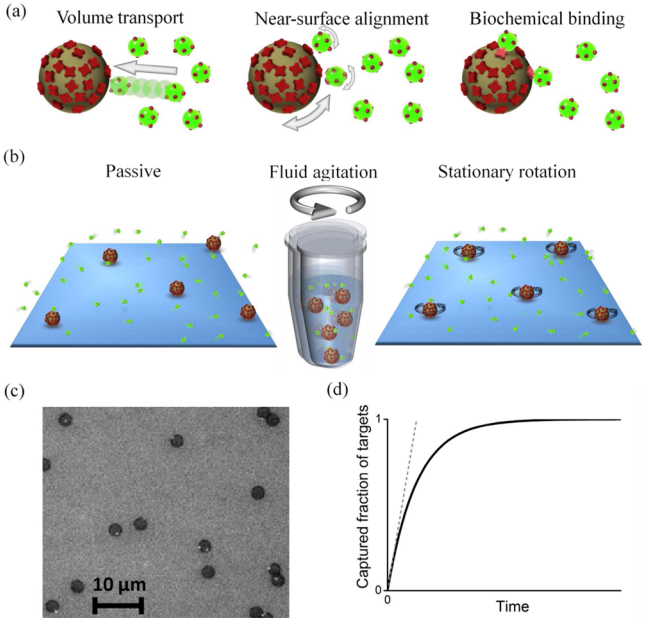

Figure 1. Principle of particle-based target capture and experimental approach. (a) Schematic representation of the different stages in the capture process of targets (in green) by capture particles (in gray). Targets and capture particles are sketched with multiple binding sites (in red). The stages are as follows: (i) volume transport creates target-particle encounters, (ii) near-surface transport creates alignment of binding sites, and (iii) bonds are formed by chemical reaction. (b) Schematic representation of the applied actuation methods: (i) passive transport by thermal diffusion, without any additional actuation, (ii) fluid agitation by vortex mixing, and (iii) magnetic rotation of the capture particles. (c) Microscope image of biotinylated fluorescent nanoparticles (200 nm) captured by streptavidin-coated microparticles (2.8 μm) on a glass surface. Single bound targets are identified and counted as the reaction proceeds. (d) Sketch of the captured fraction of targets as a function of time. The reaction rate constant is deduced from the initial slope (dashed line) or from the exponential time constant.

formed after encountering, is often named the encounter (or transient) complex. On the basis of this reaction scheme, the overall rate constant of association k_a is given by:

$$k_a = k_{enc}\frac{k_c}{k_{sep} + k_c} \tag{2}$$

Note that k_a equals the product of the encounter rate constant, k_{enc}, and the probability that the chemical reaction will subsequently occur, $[k_c/(k_{sep} + k_c)]$. In case the chemical reaction is fast relative to the separation of the encounter complex ($k_c \gg k_{sep}$), the association rate constant is limited by the encounter rate constant, so $k_a \approx k_{enc}$. In case the separation is much faster than the chemical reaction ($k_{sep} \gg k_c$), then the chemical reaction becomes rate limiting and $k_a \approx k_c K_{enc}$, with $K_{enc} = k_{enc}/k_{sep}$ the equilibrium constant for forming the encounter complex.

As Schreiber et al.,[10] have noted for protein association kinetics, there is no simple test to determine whether the encounter or the chemical reaction step is rate limiting. But it is known that encounter (i.e., diffusion) limited rate constants are typically high, i.e., above 10^5 M^{-1} s^{-1}, as is for instance the case for the streptavidin–biotin complex[13] and for typical antibody–antigen complexes,[12] and that within these reactions only local conformational changes occur. In contrast, reaction-limited protein associations generally involve gross molecular changes like loop reorganization and domain movement.

Several theoretical studies have been performed to determine the association rate constants for diffusion limited reactions. In the case of two uniformly reactive spheres with immediate binding (i.e., hit-and-stick behavior) Smoluchowski[14] found by solving the diffusion equation:

$$k_{enc}|^{dif} = k_{dif} = 4\pi DR \tag{3}$$

Here, D and R represent, respectively, the relative translational diffusivity and the center-to-center distance of the spheres when in contact ($R = R_1 + R_2$, with R_1 and R_2 the radii of the two respective spheres). The units of k_{dif} are m^3s^{-1}. For two protein-sized spheres, eq 3 predicts rate constants in the order of 10^9 M^{-1} s^{-1}, which is much larger than what is typically observed for protein molecules (10^5–10^7 M^{-1} s^{-1}).[10] It has been shown theoretically[10,15] that the reduction can be attributed to the required alignment of the position and relative orientation of the reactive binding sites on the proteins.

In analogy to the binding reaction between two proteins, the binding of two particles with distributed binding sites (as in Figure 1a) should be viewed as a multistep process, namely first translational volume transport to create encounters of the reacting particles (FT||MC), and thereafter particle movements to achieve near-surface alignment of the reactive binding sites on the particles (FT···MC):

$$\mathrm{FT} + \mathrm{MC} \underset{k_{sep}}{\overset{k_{enc}}{\rightleftarrows}} \mathrm{FT}||\mathrm{MC} \underset{k_{misalign}}{\overset{k_{align}}{\rightleftarrows}} \mathrm{FT}\cdots\mathrm{MC} \underset{k_{-c}}{\overset{k_c}{\rightleftarrows}} \mathrm{FTMC} \tag{4}$$

In this equation all rate constants have units s^{-1}, except for k_{enc} which has units M^{-1} s^{-1}. Here we have introduced the near-surface alignment rate constant, k_{align}, and in the backward direction the near-surface misalignment rate constant, $k_{misalign}$. In case the chemical reaction is much faster than alignment process ($k_c \gg k_{align}$), the overall rate constant of association is given by:

$$k_a = k_{enc}\cdot\frac{k_{align}}{k_{sep} + k_{align}} = k_{enc}p_{align} = k_{enc}\frac{K_{enc}k_{align}}{k_{enc} + K_{enc}k_{align}} \tag{5}$$

We have defined p_{align} as the probability to reach alignment during an encounter. The righthand side of eq 5 can also be obtained by solving the diffusion equation of two uniformly reacting spheres with a partially adsorbing surface and an intrinsic rate constant $\kappa \equiv K_{enc}k_{align}$ (see also Collins and Kimball,[16] who derived a similar equation for the reaction scheme in eq 1).

The rate J at which targets are captured is proportional to the overall association rate constant:

$$J = \frac{\mathrm{d[FTMC]}}{\mathrm{d}t} = k_a[\mathrm{FT}][\mathrm{MC}] \tag{6}$$

For short times, the reaction product increases linearly in time:

$$[\mathrm{FTMC}] = k_a[\mathrm{FT}]_{t=0}[\mathrm{MC}]_{t=0}t \tag{7}$$

For longer times, the concentration of one or both species may become depleted, causing a decrease in the reaction rate. More specifically, in case the number of capture particles is much larger than the number of target particles, then the concentration of unbound targets [FT] decreases over time and the amount of captured targets evolves as follows:

dx.doi.org/10.1021/jp307862h | J. Phys. Chem. B 2013, 117, 1210–1218

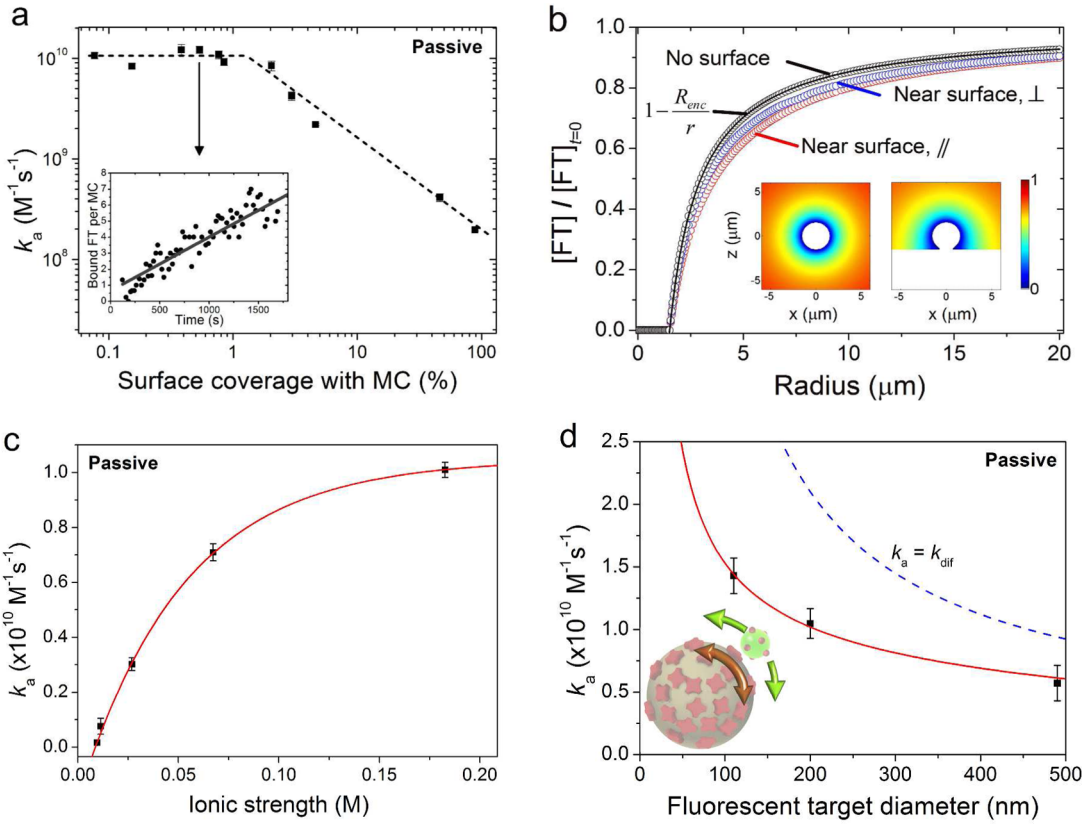

Figure 2. Quantification of passive target capture. (a) Overall reaction rate constant for different densities of magnetic capture particles (MC) on the glass substrate. The dashed line is a guide to the eye. Each data point is collected from a time-dependent measurement of target binding, as depicted in the inset. A linear fit (solid line in the inset) is used to determine the overall reaction rate constant, according to eq 7 and including a factor two to correct for measuring one hemisphere of the particle. (b) Steady-state concentration profiles of an absorbing sphere for different system geometries: dispersed in an infinite medium in the presence or absence of a nonabsorbing surface. The circles as well as the insets correspond to computations using Comsol Multiphysics. The profiles are plotted with respect to the center of the particle. The solid line represents the analytical steady-state solution of the diffusion equation. (c) Reaction rate constant for different ionic strengths of the solution. As a guide to the eye, the data is fitted using a curve of the form $y(x) = y_0[1 - \exp(A(x - x_0))]$. (d) Reaction rate constant for different sizes of the fluorescent targets. Each data point represents three measurements. The dashed line represents the theoretical rate constant in case the intrinsic rate constant κ is much larger than the encounter rate constant k_{enc}. The solid line corresponds to the model described with eq 5 (right side), using $K_{enc}k_{align} = C_1R_{MC}^{-3} + C_2R_{FT}^{-1}$, in which C_1 and C_2 are fit parameters.

$$[\mathrm{FTMC}] = [\mathrm{FT}]_{t=0}(1 - \mathrm{e}^{-t/\tau}) \quad \text{with} \quad \tau = (k_a[\mathrm{MC}]_{t=0})^{-1} \tag{8}$$

In our experiments, we could optically distinguish the first three states described in eq 4. In the free state (left) the particles are optically clearly separated. When the particles form an encounter complex, a gap between the particles cannot be optically resolved but the particles are still mobile with respect to each other. In the latter two states the particles are in contact and not anymore mobile with respect to each other. We note that biochemical dissociation does not play a role in our experiments, due to the strong binding that occurs between the particles.

EXPERIMENTAL SECTION

Particles and Chemicals. Superparamagnetic particles (M270, either carboxylated or streptavidin coated, 2.8 μm diameter) were purchased from Dynal Biotech. Fluorescent particles (Fluospheres, carboxylated, yellow/green, 0.2 μm) were purchased from Invitrogen. EZ-link biotin-PEO_3-amine was obtained from Pierce. Antibiotin antibodies and streptavidin were obtained from Thermo scientific. Fluorescent particles were coated with biotin using standard EDC coupling chemistry. Centrifugation at 14,000 rpm in a centrifuge was carried out to separate the fluorescent particles from unbound biotin. The ζ-potential of the biotinylated fluorescent particles and M270 streptavidin magnetic particles was measured using a Malvern Zetasizer nano ZS. The ζ-potential was ∼−22 mV and ∼−15 mV respectively.

Carboxylated magnetic particles were coated with either streptavidin or antibiotin antibodies using standard EDC-NHS coupling. To control the loading of streptavidin on the particles, BSA was coated competitively at different concentrations, i.e., 0.0005, 0.005, 0.05, or 0 mg BSA/mL in combination with 0.5 mg/mL streptavidin. The relative streptavidin loading was verified by means of enzyme-linked immunosorbent assay (ELISA) using biotin-HRP. The luminescence signal was measured using a Fluoroskan Ascent FL and the data is shown in Figure 1S in the Supporting Information.

Passive Transport Experiment. Stock solutions of magnetic capture particles (6.7×10^8 particles/mL) and fluorescent target particles (4.55×10^{12} particles per mL) were diluted respectively 200 and 30 times in PBS containing 0.1% BSA. A glass substrate with a spacer (height 100 μm) was

dx.doi.org/10.1021/jp307862h | J. Phys. Chem. B 2013, 117, 1210−1218

prepared and 0.5 μL of magnetic particle solution was pipetted on the substrate. Subsequently, a 9 μL droplet containing fluorescent particle solution was pipetted in the cell. The fluid cell was closed with a glass coverslip and placed under the microscope (Leica DM6000) with a 63× immersion objective lens for analysis. The magnetic particles sediment to the surface within a minute. The surface was scanned for magnetic particles and of each particle a picture was taken using an EM-CCD camera (Andor Solis) and the corresponding time was recorded. Afterward, the images were processed to count both the number of capture particles and captured target particles.

Fluid Agitation by Vortex Mixing. Solutions containing fluorescent as well as magnetic particles were mixed together in an Eppendorf tube so that the final concentration of fluorescent particles was ∼600 particles/μL. The final volume was 200 μL. These tubes were placed on a shaker (Eppendorf Thermomixer Comfort) at 1400 rpm. At several times, a small fraction of 8 μL was extracted from the tubes in order to evaluate the capture efficiency. These small volumes were pipetted into a fluid cell and analyzed under the microscope. To increase the number of magnetic microparticles within one field-of-view (142 × 107 μm^2), a ferromagnet was used to concentrate sedimented particles on the bottom center of the fluid cell. Typically, five images were recorded with 700−1300 magnetic particles inside the field-of-view.

Magnetic Rotation. Magnetic particles were rotated using a quadrupole electromagnet.[17] The four electromagnets were powered with sinusoidal currents at different phase lags such that a horizontal continuously rotating magnetic field was created at the center where the sample was placed. The magnet generates only a very small vertical field gradient, giving a force on the particles on the order of the gravitational force. The horizontal gradient was insignificant since the particles were not observed to translate horizontally in the magnetic field. In a typical experiment, the sample was prepared and placed under the microscope, and after approximately 60 s, the rotating magnetic field was started and measurements were performed.

RESULTS AND DISCUSSION

Capturing Particles by Passive Diffusive Transport. The reference method for target capturing is an experiment without any actuation, so that the transport is driven only by thermal diffusion. We have measured the corresponding reaction kinetics by recording the capture of fluorescent targets by magnetic particles sedimented on a glass substrate, as sketched in the left panel of Figure 1b. Only the top hemisphere of the magnetic capture particles was monitored, i.e., the side that is exposed to the bulk fluid, as shown in Figure 1c; we therefore included a factor of 2 in calculating the reaction rate constants per capture particle. The capture process was monitored for about 25 min (see the example in the inset of Figure 2a) and the overall association rate constant was determined using eq 7. We verified that the capture process did not significantly alter the concentration of fluorescent target particles in solution (the amount of captured target particles was always much smaller than the total amout of target particles in solution) and neither the reaction surface of capture particles (the target particles never saturated the binding area of the capture particles); see the Supporting Information.

We have studied the association rate as a function of the density of magnetic particles on the surface expressed as the surface coverage, see Figure 2a. For low surface coverage (<1.4 ± 0.6%) the association rate is found to be independent of the surface coverage and the capture curves (see inset) are linear over the measured time-span. This is the regime wherein target transport to the capture particles is dominated by radial diffusion. For higher surface coverage, the amount of captured targets increases over time in a sublinear fashion, namely as $t^{1/2}$ (not shown). This behavior corresponds to a system with an absorbing plane and a diffusion-limited supply of targets, as is shown and discussed in the Supporting Information. The data in the regime of high surface coverage (>1.4% capture particles on the glass substrate) corresponds to the average reaction rate over the measured time-span. The average reaction rate constant is found to decrease with an increasing density of capture particles on the surface, which is caused by overlap of target depletion zones that are formed around capture particles.[18] An overlap of depletion zones of neighboring particles results in a shift from radial to linear symmetry of the transport process, causing a decrease of the supply of targets per capture particle and therefore a decrease of the encounter rate. The decrease of the reaction rate per capture particle should occur when the diffusion length is comparable to the distance between the particles. For these measurements, we estimate that $L_{avg} \sim 0.5(Dt)^{1/2} \sim 28$ μm, corresponding to a surface coverage of ∼0.9%, which is in agreement with our measurements. In the regime of high surface coverage (>1.4%) the average rate constant scales as the inverse of the surface coverage, see the Supporting Information. In this regime the total amount of captured targets is independent of the number of capture particles, which is in agreement with the interpretation that the system acts as an effective absorbing plane for target particles and that the number of capture particles is irrelevant.

In the regime of radial transport, the overall rate constant of association is found to be $k_a = 1.0 \pm 0.2 \times 10^{10}$ M^{-1} s^{-1} (see Figure 2a). Interestingly, the measured rate constant is significantly smaller than the calculated association rate constant for a diffusion limited reaction [see eq 3]: $k_{dif} = 2.4 \times 10^{10}$ M^{-1} s^{-1}. This means that an additional process is limiting the reaction. In order to unravel the origin of the limiting process, we will now analyze (i) the influence of the planar glass substrate on the measured association rate, (ii) the influence of electrostatic repulsion between the particles, (iii) the influence of the size of the targets, and (iv) the influence of the biological molecules on the particles.

Influence of the Planar Substrate. Targets do not adsorb to the planar glass substrate, but the presence of the substrate may still limit the supply of targets to the capture particles. Finite-element simulations were carried out using Comsol Multiphysics 3.5a to compute the steady-state concentration profiles for a sphere in an infinite medium and a sphere near a nonabsorbing surface, see Figure 2b. We have also calculated the steady-state concentration profile by analytically solving the diffusion equation for an absorbing sphere with an encounter radius $R_{enc} = R_{MC} + R_{FT} = 1.5$ μm in an infinite medium (see the solid line). The numerical solution in case of an absent surface shows excellent agreement with the analytical solution. The computations show that the presence of a nonabsorbing surface slightly decreases the target concentration compared to the situation when no surface is present. From the computations, we can derive the diffusive flux of targets at the encounter radius of the top hemisphere. We find that the nearby nonabsorbing surface causes a decrease of the encounter rate by 13% ($\varepsilon = 0.133 \pm 0.001$). Therefore, we conclude that

dx.doi.org/10.1021/jp307862h | J. Phys. Chem. B 2013, 117, 1210−1218

the nearby nonabsorbing surface has only a minor effect on the overall rate constant of association.

Influence of Electrostatic Interactions. The target as well as the capture particles have a negative surface charge (see Experimental Section) so electrostatic repulsion may play a role in limiting the overall association rate. The electrostatic repulsion between the particles was studied by varying the ionic strength of the buffer solution, namely by diluting the PBS buffer from physiological concentration (~0.18 M) down to ~0.01 M, see Figure 2c. The reaction rate increases as a function of the ionic strength and saturates near the physiological concentration. Therefore, we conclude that the electrostatic repulsion is nearly completely screened at physiological salt levels. We can compare these findings to calculations by DLVO theory[19] (see Supporting Information). For the 0.01 M solution, the combination of electrostatic repulsion and van der Waals attraction gives an energy barrier with a height of $\sim 10 k_B T$, and the $1 k_B T$ energy level is reached at an interparticle gap of 12 nm between target and capture particle. For the 0.18 M solution, there is no net energy barrier, caused by the screening of the electrostatic interaction by the high salt concentration. Therefore, the experiments and calculations indicate that electrostatic interactions are not expected to be a limiting factor in the association rate between particles suspended in undiluted PBS.

The Influence of the Size of the Targets. The overall rate constant of association was measured for three different sizes of the target particles, as shown in Figure 2d. The graph also shows the calculated diffusion-limited rate constant in case of immediate binding between the particles, i.e. a hit-and-stick behavior, as expressed by eq 3. For all sizes, the measured association rate (k_a) is lower than the diffusion-limited hit-and-stick rate (k_{dif}). This indicates that an additional process reduces the binding probability after an encounter between particles. As discussed earlier, the limiting process might be the chemical reaction, or the process of near-surface alignment of the binding sites to enable the chemical reaction. Since the binding affinity of streptavidin to biotin is high, and as the particles contain many streptavidin/biotin molecules on their surfaces, it is not the chemical reaction that limits the target capture rate (data will be shown in the next paragraph).

Figure 2d shows that the ratio between k_{dif} and k_a depends not strongly on the size of the targets: the ratio is about a factor 2.5 for the 100 nm targets and about 1.5 for the 500 nm targets. So let us now develop a description of the target size dependence of the overall association rate, starting from eq 5. The encounter rate k_{enc} is given in eq 3 and is proportional to the diffusivity (Stokes−Einstein relationship, proportional to $1/R$) and the radii of the particles (R). In our system the two particle types have strongly unequal radii: $R_{MC} \gg R_{FT}$. Therefore, the encounter rate k_{enc} is proportional to R_{MC}/R_{FT}. As separation is diffusive, the separation rate k_{sep} is proportional to $1/R_{FT}$.

To reach near-surface alignment of the binding sites, it is required that a binding site on the target particle comes in the vicinity of a binding site on the capture particle. In other words, binding sites of both particles must be present in the interaction area, in between the particles. The process of near-surface alignment involves the mutual surface scanning and probing of the two particles, which can have contributions from translational as well as rotational processes (see the inset of Figure 2d). The processes can be thermally excited (Brownian motion) or can be driven by an applied excitation (magnetic or fluidic actuation). A full theoretical analysis of these coupled processes is outside the scope of this paper; instead we follow a heuristic approach in order to come to scaling relationships with the radii of the particles.

Concerning the contribution of translational transport to the near-surface alignment process, we expect that the alignment rate is determined by the fastest particles, so by the target particles, with a displacement scaling as $1/R_{FT}$. Concerning rotation, the time required for rotational randomization scales with the third power of the radius ($\sim 1/R^3$) and equals the time needed for Brownian diffusion over a distance of the diameter of the particle.[20] In water, the time required for total rotational randomization is 3×10^{-6} s for biomolecules with a size of 10 nm, 3 ms for a 100 nm sized particle, 3 s for particles or cells with a size of 1 μm, and 3000 s for cells with a size of 10 μm. In view of the observed weak dependence of k_{dif}/k_a on target size (see Figure 2d), we conclude that the rotation of the target particles (scaling as $1/R_{FT}^3$) is not a dominant limiting factor in the experiment.

Interestingly, the Brownian rotation of the capture particles generates surface displacements that are of similar magnitude as the translational diffusion of the target particles (see the inset of Figure 2d). For example, during a time-span of 0.1 s, the root-mean-square displacement by translational diffusion of a free 200 nm target particle in water is ~0.6 μm; and the root-mean-square displacement of the outer surface of the capture particle due to rotational diffusion is ~0.2 μm. These values show that the diffusive translation of the target particle and the rotational diffusion of the capture particle are expected to contribute roughly equally to the process of near-surface alignment. Therefore, we propose a dependence of the near-surface alignment rate on the particle radii of the form:

$$k_{align} \cong C_1 R_{MC}^{-3} + C_2 R_{FT}^{-1} \quad (9)$$

Applying this equation in the right-hand side of eq 5, and using $k_{enc} = k_{dif,surf} = (1 - \varepsilon) k_{dif}$, to the data in Figure 2d, we find a good fit with $K_{enc}C_1 = (2.9 \pm 0.7) \times 10^{-8}$ $M^{-1}{\cdot}m^3{\cdot}s^{-1}$ and $K_{enc}C_2 = (10 \pm 3) \times 10^2$ $M^{-1}{\cdot}m{\cdot}s^{-1}$. Interestingly, both contributions to the alignment rate are found to be on the same order of magnitude.

From the experimental data and the model, we conclude that near-surface alignment is indeed a limiting factor in the process of target capture. The capture process starts with volume transport driven by translational diffusion, and subsequently near-surface alignment is required to enable a chemical reaction between the molecules on the surfaces of the particles. Near-surface alignment is distinctly different from volume transport in that rotational diffusion plays an important role.

It would be interesting to directly measure the rotational processes in the experiment. The fluorescent target particles studied in this paper have a rotational randomization time on the order of a few tens of milliseconds. This time is much smaller than the interframe time in the experiment (~10 fps give an interframe time of ~100 ms). So we conclude that we are not able to record in detail the particle dynamics during a single encounter due to the limited frame rate in the present experimental setup. For further studies either a more light sensitive high speed camera is needed or a different technique may be used such as fluorescence correlation spectrometry.

Influence of the Biochemical Binders. We have studied the influence on the association rate of the biochemical binding molecules that are coupled to the surfaces of the particles.

dx.doi.org/10.1021/jp307862h | J. Phys. Chem. B 2013, 117, 1210−1218

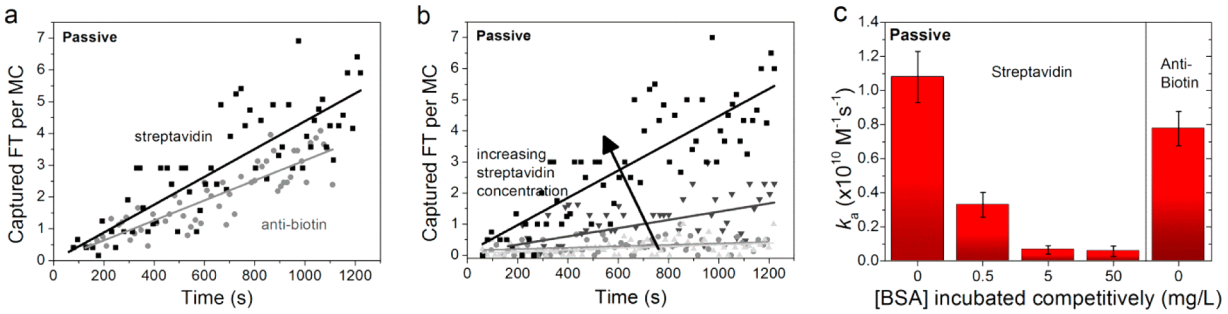

Figure 3. Influence of the surface functionalization of the capture particles on the reaction rate. (a) Capture of biotinylated targets by microparticles coated with streptavidin (■) or with antibiotin (●). The lines represent linear fits of the data. (b) Capture of biotinylated targets by microparticles with different streptavidin surface densities. (c) Overall rate constant of association k_a is shown for streptavidin and antibiotin capture proteins and different loading of streptavidin. As a measure for the streptavidin loading, the concentration of BSA is shown which was incubated simultaneously during the coating with capture proteins (also see Experimental Section and Figure 1S in the Supporting Information).

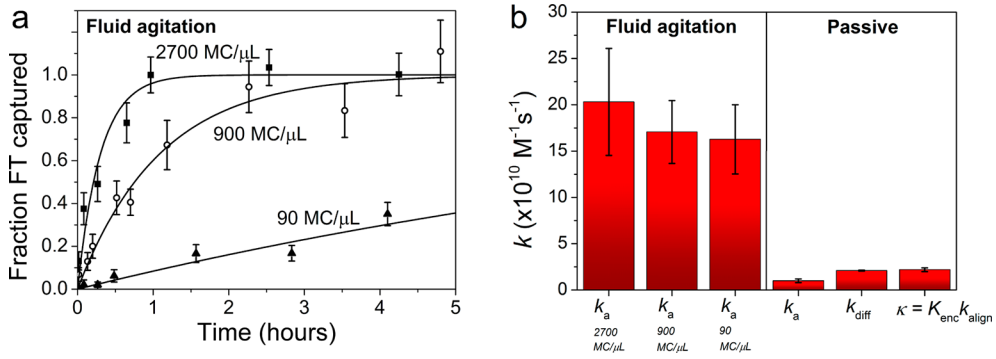

Figure 4. Quantification of target capture by fluid agitation. (a) Target capture during actuation by means of vortex mixing. Different concentrations of magnetic particles (MC) were studied. A fit based on eq 8 was used to determine the overall rate constant of association. (b) Overall rate constant of association, in case of fluid agitation with different concentrations of MC (left) and for passive target capture (right).

Passive transport experiments were performed with streptavidin or with antibiotin antibodies as the molecules on the capture particles, see Figure 3. Both molecules are good binders, but streptavidin has a 10−100 times higher reported association rate to biotin than antibiotin: about 10^8 M^{-1} s^{-1} for streptavidin[13,21] versus 10^6 to 10^7 M^{-1} s^{-1} for antibiotin.[12] Interestingly, in our particle-based experiments we find only a very small difference (factor 1.4 ± 0.3) in the association rate constant for streptavidin versus antibiotin coated capture particles, see Figure 3a. We have also studied the overall reaction rate constant for different amounts of streptavidin on the capture particles. The streptavidin density on the particles was reduced by competitive coating of carboxyl particles with streptavidin and BSA (see Experimental Section). The reduced streptavidin loading of the particles was qualitatively confirmed by ELISA measurements, as shown in Figure 1S in the Supporting Information. For different streptavidin densities, we monitored the capture reaction in a passive target capture experiment (see Figure 3b). We observe a strong dependence of the reaction rate constant on the streptavidin loading, as is shown in Figure 3c. We attribute the decrease of the association rate with decreasing streptavidin density to the fact that the association rate is limited by near-surface alignment. The data show that the overall rate constant of association hardly depends on the bond type but does depend on the density of available binding sites on the capture particles. Therefore, we conclude that mainly near-surface alignment reduces the binding probability upon encounter, and not the chemical reaction.

Fluid Agitation by Vortex Mixing. The effect of fluid agitation on the overall rate constant of association was studied by applying vortex mixing. The amount of formed FTMC complexes was determined as a function of time by extracting a small amount of fluid from the reaction mixture at different times and by counting the number of capture particles and captured targets. We employed target concentrations of ~1 fM, which is substantially lower than the concentrations used in the experiments without fluid agitation (0.8 pM). The reason for using a very low concentration is to prevent multiparticle clustering during the experiment.

Target capture was measured for different concentrations of magnetic particles (see Figure 4a). Because of the low concentration of targets, a depletion of targets from the whole sample volume was observed over time, in agreement with eq 8. The corresponding fits give values for k_a as shown in Figure 4b. The average overall rate constant of association when applying fluid agitation was found to be $k_a = 17.5 \pm 1.5 \times 10^{10}$ M^{-1} s^{-1}. This is more than an order of magnitude higher than the association rate constant that we found in the case of passive transport, i.e. $1.0 \pm 0.2 \times 10^{10}$ M^{-1} s^{-1}. The association rate constant also exceeds the intrinsic rate constant that was determined in passive experiments with the same capture particles, i.e., $\kappa = K_{enc}k_{align} = 2.1 \pm 0.2 \times 10^{10}$ M^{-1} s^{-1}. Consequently, fluid agitation enhances not only the frequency at which target particles and capture particles encounter, but it also enhances the probability that particles bind during an encounter, by at least a factor of 9 ± 2. These results also support the hypothesis that the chemical reaction rate constant

dx.doi.org/10.1021/jp307862h | J. Phys. Chem. B 2013, 117, 1210−1218

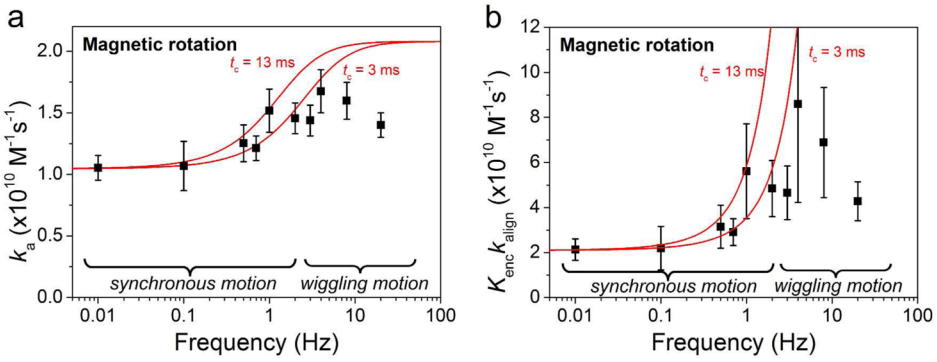

Figure 5. (a) Overall rate constant of association k_a for capture particles that rotate on a glass surface, measured as a function of the rotation frequency of the applied field. The amplitude of the applied field was 5 mT. Up to ~1.5 Hz, the particles exhibit synchronous rotations, and above ~1.5 Hz wiggling motion is observed. The lines correspond to the combination of eqs 5 and 10, with t_c the average lifetime of the encounter complex. (b) Corresponding intrinsic rate constant $\kappa = K_{enc}k_{align}$ has been determined using eq 5 and assuming no rate limitations due to the chemical reaction. The lines correspond to the model of eq 10.

is not a limiting factor, as the chemical reaction cannot be enhanced by physical transport processes. We hypothesize that by applying fluid agitation, the mobility of a target during an encounter is increased, such that a larger surface area is probed for possible binding sites as compared to diffusive transport. As a result, the binding probability for each encounter is increased. To test this hypothesis in a more controlled manner, we have also used magnetic fields to rotate the magnetic capture particles during the reaction.

Actuation by Stationary Magnetic Rotation. We have studied the effect of rotation of the capture particles on the association rate constant. The experiments were performed in the same way as passive transport experiments, but now a magnetic field was applied rotating in the same plane as the surface on which the magnetic particles were sedimented. A rotating magnetic field causes the superparamagnetic particles to rotate, caused by a small ferromagnetic moment in the particles.[22] For a more detailed characterization and description, see the Supporting Information. Because of the very small Reynolds number for this system, i.e. Re < 10^{-4} for a 1 Hz rotation, viscous forces dominate the fluid flow, and therefore no radial transport of targets is induced by the particle rotation. As verification, we have numerically compared radial transport by diffusion with radial transport induced by particle rotation (see Supporting Information).[23] From this estimation, we find that diffusive transport has a contribution to the radial target transport that is at least a factor 500 times larger as compared to induced fluid flow. Consequently, the target transport toward the capture particles is governed by diffusion and the particle rotation only affects the particle-to-target near-surface alignment process.

In Figure 5a, the overall rate constant of association, k_a, is shown as a function of the rotation frequency of the magnetic field. At low frequencies k_a equals the value for passive transport. For increasing frequencies an increase of the association rate constant is observed, and above 1 Hz the association rate constant saturates. We can understand this saturation behavior from the rotation characteristics of the particles (see the Supporting Information). The particles synchronously follow the rotating field up to a frequency where the hydrodynamic drag becomes higher than the magnetic torque, i.e. at about 1.5 Hz. Above this critical frequency the particles do not completely follow the rotating magnetic field anymore and assume a wiggling motion with a lowered net rotation frequency. Our data show that the wiggling motion is still effective for enhancing the capture process, generating a k_a with a value of about $1.5 \pm 0.2 \times 10^{10}$ M^{-1} s^{-1}. For much higher frequencies the particle rotation association rate should return to the passive transport value, but this is not visible in the graph because 20 Hz was the maximum frequency that could be applied with the magnet.

As no additional radial transport of targets is realized, the increase in reaction rate constant must be due to an enhanced near-surface alignment probability. Using eq 5 and assuming that the chemical reaction is not limiting, we have determined the intrinsic rate constant for different rotation frequencies, as shown in Figure 5b. The applied rotation clearly causes more targets to associate to the capture particles.

It is interesting to see whether we can apply the scaling relationship for the particle size dependence of the association rate, as proposed in eq 9. In case of applied magnetic rotation, the first term of eq 9 ($C_1R_{MC}{}^{-3}$) should be altered because that term relates to the rotational motion of the capture particle. The $R_{MC}{}^{-3}$-character stems from the rotational viscous drag term in the rotational diffusion constant of the capture particle, $D_{rot,MC}$. Because of the magnetically driven rotation with angular velocity ω, the root-mean-square rotation is effectively enhanced: $\theta_{rms} \rightarrow \theta_{rms}{}^* = \theta_{rms} + \omega \cdot t_c$. Here t_c is the average lifetime of the encounter complex in case the chemical reaction does not proceed. From the separation rate constant, we estimate that the average lifetime of the encounter complex is in the range of 3 to 13 ms (see the Supporting Information). Consequently, we include additional rotation in eq 9 as:

$$k_{align} \cong C_1 R_{MC}{}^{-3} \frac{D_{rot,MC} + \sqrt{t_c D_{rot,MC}}\,\omega + 4^{-1} t_c \omega^2}{D_{rot,MC}} + C_2 R_{FT}{}^{-1} \qquad (10)$$

which for $\omega \rightarrow 0$ reduces to eq 9. We have neglected the influence of the applied magnetic field on the rotational diffusion itself, because the external magnetic field has only a minor influence on the rotational Brownian diffusion during an encounter (see the Supporting Information). Using the estimated lifetime of the encounter complex and the earlier found values for the constants C_1 and C_2 (see Figure 2d), we can calculate the dependence of the association rate constant on the particle angular velocity, which is plotted in Figure 5. We find that the values are indeed in agreement with the

dx.doi.org/10.1021/jp307862h | J. Phys. Chem. B 2013, 117, 1210−1218

experimental data for frequencies up to a few hertz, whereafter the synchronous rotational motion stops and is replaced by a decreasing wiggling motion of the particles.

The results in Figure 5 show that the process of near-surface alignment limits the capture rate and not the biochemical association, which is consistent with the data reported in Figure 2 and Figure 3. Furthermore, by applying a heuristic model description of the near-surface alignment process (eqs 9 and 10), we find that the translation of the target particles and the rotation of the capture particles are important factors contributing to the near-surface alignment.

CONCLUSIONS

We have presented a detailed study on target capture using biochemically coated microparticles. Three different types of actuation were employed and the corresponding reaction rate constants were determined by quantifying the reaction kinetics with single target resolution. With respect to passive target capture, fluid agitation affects the overall rate constant of association in two ways. Fluid agitation increases the encounter rate of target and capture particles (volume transport), and interestingly, it also increases the probability of binding during an encounter (near-surface alignment). Continuous rotational actuation of capture particles also provides an increase in the overall rate constant, but not in the encounter rate, so rotation generates an increase of the binding probability or the near-surface alignment rate when particles encounter. The increase in binding probability is attributed to a combination of enhanced displacement and reorientation near the reactive surface, which increases the probability that binding sites align. We have shown that for our model system with 200 nm sized targets, the overall rate constant of association can be increased by a factor of at least 18 ± 5 by applying fluid agitation, representing a significant acceleration of target capture by both volume transport and near-surface alignment processes.

We have obtained the above insights from model experiments with nanoparticle targets, with binding via biotin/streptavidin and biotin/antibiotin, and with buffer solutions. Yet the field of particle-based target capture is much broader, with the targets ranging from small molecules to large cells, with molecular capture moieties ranging from strong binders to weak binders, and with the fluids ranging from simple buffers to complex matrices such as blood and saliva. Now let us discuss the follow-up questions that are raised by the results of this paper.

Cells are large and diffuse slowly, so both volume and near-surface transport will be limiting the reaction rate constant. Molecular targets are small and diffuse relatively fast. Yet diffusive motion is random and therefore translation over large distances is relatively inefficient. Locally, the diffusive translation and rotation of molecules is very efficient. Therefore, for molecular targets the near-surface translation and rotation after an encounter will be less limiting to the overall reaction in comparison to the volume transport that is required to generate the encounters.

Concerning the fluid matrix, in this study we have employed solutions with a viscosity close to water. In real-life situations the biological targets may be captured from complex matrices such as blood or saliva, which have higher viscosities. A higher viscosity will slow down the transport in the fluid as the viscous drag is increased, and as a consequence both volume transport and near-surface alignment will become even more limiting with respect to the chemical reaction.

Our results shed light on the underlying processes determining the overall association rate in biochemical particle-based target capture. The insights are particularly important for the development of target capture methods for small microliter-sized sample volumes. In small sample volumes, global mixing by mechanical vortexing cannot be applied, because global mixing requires relatively large fluid volumes, i.e., at least on the order of 100 μL. For small volumes novel actuation methods need to be developed, e.g., based on active particle rotations and displacements. For such purposes magnetic particles are particularly advantageous as they can be manipulated with relative ease using externally applied magnetic fields.

In summary, we have presented a comprehensive methodology to quantify contributions of volume transport, near-surface alignment and biochemical association to the rate constants of particle-based target capture. Our results consistently highlight the importance of volume transport and near-surface alignment and pave the way for a range of further studies on the acceleration of particle-based target capture and for the development of ultrahigh-sensitive technologies for the analysis of small sample volumes.

ASSOCIATED CONTENT

Supporting Information

Characterization of relative loading of streptavidin on magnetic particles, losses in target concentration or reactive surface of capture particles, target capture at high surface coverages, estimating DLVO interaction energies, characterization of the response of magnetic particles in a rotating field, estimating radial transport, estimating the lifetime of an encounter complex, and Brownian rotation of a capture particle in an external magnetic field. This material is available free of charge via the Internet at http://pubs.acs.org.

AUTHOR INFORMATION

Corresponding Author

*E-mail: a.v.reenen@tue.nl.

Notes

The authors declare no competing financial interest.

ACKNOWLEDGMENTS

We thank Hans van Zon for critical reading of the manuscript. This project was funded by the Dutch Technology Foundation (STW) under Grant 10458.

REFERENCES

(1) Sieben, S.; Bergemann, C.; Lubbe, A.; Brockmann, B.; Rescheleit, D. *J. Magn. Magn. Mater.* **2001**, *225*, 175−179.

(2) Kielhorn, E.; Schofield, K.; Rimm, D. L. *Cancer* **2002**, *94*, 205−211.

(3) Bruls, D. M.; Evers, T. H.; Kahlman, J. A. H.; van Lankvelt, P. J. W.; Ovsyanko, M.; Pelssers, E. G. M.; Schleipen, J. J. H. B.; de Theije, F. K.; Verschuren, C. A.; van der Wijk, T.; et al. *Lab Chip* **2009**, *9*, 3504−3510.

(4) Sabatte, G.; Feitsma, H.; Evers, T. H.; Prins, M. W. *Biosens. Bioelectron.* **2011**, *29*, 18−22.

(5) Nam, J. M.; Thaxton, C. S.; Mirkin, C. A. *Science* **2003**, *301*, 1884−1886.

(6) Yeung, S. W.; Hsing, I. M. *Biosens. Bioelectron.* **2006**, *21*, 989−997.

(7) Boom, R.; Sol, C. J.; Salimans, M. M.; Jansen, C. L.; Wertheim-van Dillen, P. M.; van der Noordaa, J. *J Clin. Microbiol.* **1990**, *28*, 495−503.

(8) Todd, J.; Freese, B.; Lu, A.; Held, D.; Morey, J.; Livingston, R.; Goix, P. *Clin. Chem.* **2007**, *53*, 1990−1995.
(9) Rissin, D. M.; Kan, C. W.; Campbell, T. G.; Howes, S. C.; Fournier, D. R.; Song, L.; Piech, T.; Patel, P. P.; Chang, L.; Rivnak, A. J.; et al. *Nat. Biotechnol.* **2010**, *28*, 595−599.
(10) Schreiber, G.; Haran, G.; Zhou, H. X. *Chem. Rev.* **2009**, *109*, 839−860.
(11) Schurr, J. M. *Biophys. J.* **1970**, *10*, 700−716.
(12) Gabdoulline, R. R.; Wade, R. C. *Curr. Opin. Struct. Biol.* **2002**, *12*, 204−213.
(13) Arlett, J. L.; Myers, E. B.; Roukes, M. L. *Nat. Nanotechnol.* **2011**, *6*, 203−215.
(14) Smoluchowski, v. M. *Z. Phys. Chem.* **1917**, *92*, 129−168.
(15) Schmitz, K. S.; Schurr, J. M. *J. Phys. Chem.* **1972**, *76*, 534−545.
(16) Collins, F. C.; Kimball, G. E. *J. Colloid Sci.* **1949**, *4*, 425−437.
(17) Janssen, X. J. A.; van Reenen, A.; van IJzendoorn, L. J.; Prins, M. W. J. *Colloids Surf A: Physicochem. Eng. Aspects* **2011**, *373*, 88−93.
(18) Waite, T. R. *Phys. Rev.* **1957**, *107*, 463−470.
(19) Leckband, D.; Israelachvili, J. *Q. Rev. Biophys.* **2001**, *34*, 105−267.
(20) Lee, N. K.; Johner, A.; Thalmann, F.; Cohen-Tannoudji, L.; Bertrand, E.; Baudry, J.; Bibette, J.; Marques, C. M. *Langmuir* **2008**, *24*, 1296−1307.
(21) Srisa-Art, M.; Dyson, E. C.; deMello, A. J.; Edel, J. B. *Anal. Chem.* **2008**, *80*, 7063−7067.
(22) Janssen, X. J. A.; Schellekens, A. J.; van Ommering, K.; van Ijzendoorn, L. J.; Prins, M. W. J. *Biosens. Bioelectron.* **2009**, *24*, 1937−1941.
(23) Fosdick, R. L.; Kao, B. G. *Rheol. Acta* **1980**, *19*, 675−679.

■ NOTE ADDED AFTER ASAP PUBLICATION

This paper was published ASAP on January 18, 2013. The paper was reposted on January 24, 2013 with a revised title.